doi:10.1016/j.jmb.2007.08.058 J. Mol. Biol. (2007) 374, 374–383

JMB

Available online at www.sciencedirect.com

ScienceDirect

ELSEVIER

Bis-methionyl Coordination in the Crystal Structure of the Heme-binding Domain of the Streptococcal Cell Surface Protein Shp

Roman Aranda IV[1], Chad E. Worley[2], Mengyao Liu[3], Eduard Bitto[2], M. Susan Cates[4], John S. Olson[4], Benfang Lei[3] and George N. Phillips Jr[2]*

[1]*Department of Biomolecular Chemistry, University of Wisconsin-Madison, Madison WI 53706, USA*

[2]*Department of Biochemistry University of Wisconsin-Madison, Madison, WI 53706 USA*

[3]*Department of Veterinary Molecular Biology, Montana State University, Bozeman MT 59717, USA*

[4]*Department of Biochemistry and Cell Biology and W. M. Keck Center for Computational Biology, Rice University Houston, TX 77251, USA*

Received 3 July 2007; received in revised form 23 August 2007; accepted 25 August 2007
Available online 31 August 2007

Edited by M. Guss

Surface proteins Shr, Shp, and the ATP-binding cassette (ABC) transporter HtsABC are believed to make up the machinery for heme uptake in *Streptococcus pyogenes*. Shp transfers its heme to HtsA, the lipoprotein component of HtsABC, providing the only experimentally demonstrated example of direct heme transfer from a surface protein to an ABC transporter in Gram-positive bacteria. To understand the structural basis of heme transfer in this system, the heme-binding domain of Shp (Shp^{180}) was crystallized, and its structure determined to a resolution of 2.1 Å. Shp^{180} exhibits an immunoglobulin-like β-sandwich fold that has been recently found in other pathogenic bacterial cell surface heme-binding proteins, suggesting that the mechanisms of heme acquisition are conserved. Shp shows minimal amino acid sequence identity to these heme-binding proteins and the structure of Shp^{180} reveals a unique heme–iron coordination with the axial ligands being two methionine residues from the same Shp molecule. A negative electrostatic surface of protein structure surrounding the heme pocket may serve as a docking interface for heme transfer from the more basic outer cell wall heme receptor protein Shr. The crystal structure of Shp^{180} reveals two exogenous, weakly bound hemins, which form a large interface between the two Shp^{180} molecules in the asymmetric unit. These "extra" hemins form a stacked pair with a structure similar to that observed previously for free hemin dimers in aqueous solution. The propionates of the protein-bound heme coordinate to the iron atoms of the exogenous hemin dimer, contributing to the stability of the protein interface. Gel filtration and analytical ultracentrifugation studies indicate that both full-length Shp and Shp^{180} are monomeric in dilute aqueous solution.

© 2007 Elsevier Ltd. All rights reserved.

Keywords: cell surface protein; heme-binding protein; *Streptococcus pyogenes*; Shp; heme acquisition

Introduction

The ongoing emergence of antibiotic resistance in pathogenic bacteria has led to interest in resolving critical pathways that can be exploited for new drug design. The heme-uptake system is one such potential target to the dependency of a variety of bacteria on the host for essential iron.[1–4] Gram-positive pathogens, such as *Streptococcus pyogenes* and *Staphylococcus aureus*, cannot survive on the limited amounts of free iron that are available in their hosts[5] and instead use heme-binding proteins to gather iron from host proteins such as human hemoglobin from lysed red blood cells.[6–9] These bacteria have evolved transport systems to relay heme through the cell wall and translocate it across the cytoplasmic membrane.

**Corresponding author.* E-mail address: phillips@biochem.wisc.edu.

Abbreviations used: ABC, ATP-binding cassette; MW, molecular weight.

0022-2836/$ - see front matter © 2007 Elsevier Ltd. All rights reserved.

S. pyogenes is a Gram-positive bacterium that causes many human diseases, including streptococcal toxic shock, rheumatic fever, rheumatic heart disease, pharyngitis, and bacteremia.[10] *S. aureus* prefers heme as an iron source, but can use transferrin iron for growth.[8] *S. pyogenes* acquires and uses heme as an efficient iron source, but is unable to use iron bound to transferrin.[11,12] The heme acquisition machinery of *S. pyogenes* consists of Shr, Shp, and the ATP-binding cassette (ABC) transporter HtsABC. Shr is as outer surface protein that can interact with host hemoproteins.[13] Shp, another surface protein, and HtsA, the lipoprotein component of HtsABC, both bind heme avidly.[2,14] Previous *in vitro* studies have shown that Shp transfers the reduced (Fe(II)-protoporphyrin IX or heme) or oxidized (Fe(III)-protoporphyrin IX or hemin) cofactor to HtsA.[15,16] The observed rate constant for hemin transfer from Shp to HtsA shows a hyperbolic dependence on apoHtsA concentration, indicating that Shp and apoHtsA form a complex prior to hemin transfer. The limiting first-order rate constant for transfer at high protein concentrations is very large (~40 s^{-1}), roughly 10^5 times greater than that for simple hemin dissociation from holoShp (~0.0003 s^{-1}).[16] These kinetic results demonstrate that the heme transfer is direct and activated by formation of a binary holoShp–apoHtsA complex. However, little is known about the structural basis of this rapid heme transfer.

Only a few structures of the proteins involved in bacterial heme acquisition and metabolism have been described and include the *S. aureus* surface proteins IsdH, IsdC, and IsdA.[17–19] These *S. aureus* proteins belong to the NEAT-domain family of proteins and share domain homology with Shr (referred to as S_pyog in the cited reference).[20] In addition, crystal structures have also been solved for the heme uptake and metabolism proteins: *Serratia marcescens* hemophore HasA, *Campylobacter jejuni* lipoprotein ChaN, *Yersinia enterocolitica* heme transporter protein HemS, *S. aureus* lipoprotein IsdE, and *Escherichia coli* heme oxygenase ChuS.[21–25] The heme in IsdA, IsdC, and ChaN is coordinated through a tyrosine-iron linkage, and hydrophobic residues line the heme pocket. Heme bound by the transporter proteins is more exposed to the solvent than that in other heme proteins with catalytic, gas storage, and sensing functions, such as myoglobin, hemoglobin, cytochrome P450s, and guanylyl cyclase. The exposed surfaces are presumed to facilitate rapid heme transfer.

Here we report the first protein structure of a component of the heme-uptake machinery in *S. pyogenes*. The heme-binding domain of Shp (Shp^{180}) was constructed by removing the N-terminal secretion signal sequence and the C-terminal domain, which presumably attaches to the cell wall. Ran, *et al*. have shown that Shp^{180} retains the ability to bind heme and hemin avidly and to transfer these metalloporphyrins rapidly to apoHtsA by the same mechanism as that observed for full-length Shp.[26] The structure of Shp^{180} was determined in its hemin-bound state.

Results

Structure determination

The structure of Shp^{180} (Figure 1) was phased using single wavelength anomalous diffraction from a 2.6 Å resolution phasing data set collected at a wavelength near the iron K-edge. The initial model obtained from the phasing data set was refined

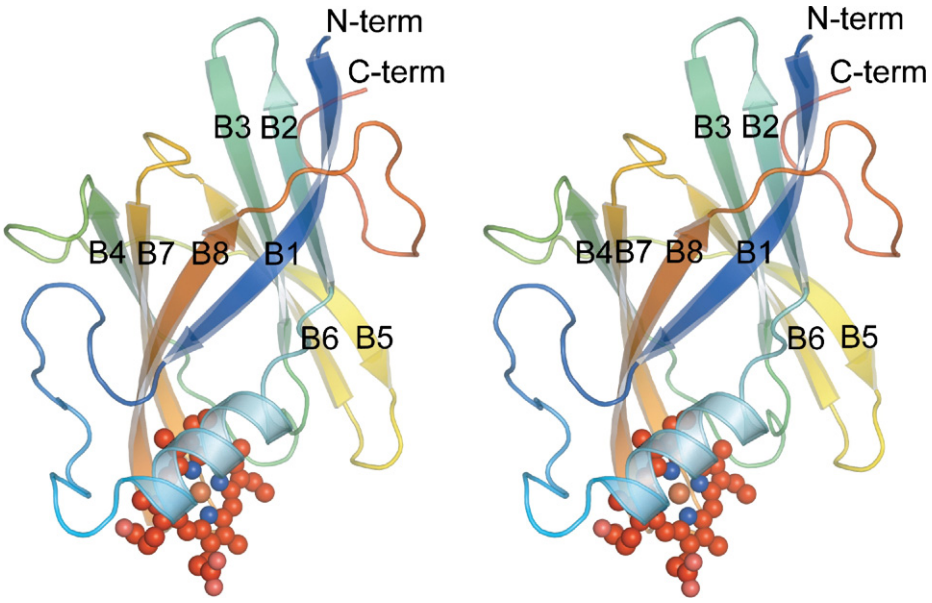


Figure 1. Shp^{180} structure. The stereo image of Shp^{180} in cartoon representation. The hemin is shown in the ball and stick model. The termini and the β-sheets are labeled.

against a high-resolution data set extending to 2.1 Å (see Table 1 for X-ray crystallization statistics). Two Shp^{180} molecules are located in the asymmetric unit, each with a single hemin bound to the protein and an exogenous hemin in the crystallization dimer interface. The two Shp^{180} monomers have a main-chain r.m.s. deviation of 0.76 Å. The largest difference between the two monomers is restricted to six residues following β-strand B8 (Figure 1). When these amino acids are excluded, the main-chain r.m.s. deviation between the monomers is reduced to 0.36 Å, demonstrating nearly identical molecules within the asymmetric unit.[27]

Structure of Shp^{180}

The immunoglobulin-like β-sandwich fold of Shp^{180} contains eight β-strands and one α-helix (Figure 1). The eight β-strands are divided into three and four-stranded antiparallel β-sheets forming a twisted β-sandwich with the eighth β-strand connecting the two β-sheets. Unlike the penta-coordinate heme in the *S. aureus* or *C. jejuni* uptake proteins, the heme in Shp is coordinated by two methionine residues (Figure 2(a)). Bis-methionyl coordination has only been documented in bacterioferritin, where the thiol ether coordination comes from methionine residues on separate monomers.[28,29] Shp^{180} is the first protein to show this arrangement within the same monomer. The bound heme iron is coordinated by Met66 and Met153, which are located on the α-helix and between β-strands B7 and B8, respectively (Figure 1). The sulfur atoms are located 2.4 Å from the iron atom for both Met66 and Met153 (Figure 2(a)), comparable to the 2.1 Å –2.7 Å distance found between monomers in structures of bis-methionyl bacterioferritin[29–31] and to the 2.3 Å average for Fe–S distances in Fe–Cys protein structures (primarily cytochrome P450s) taken from the Protein Data Bank.[32,33] Met66 is more solvent exposed than Met153, which is in agreement with IsdC where the 3_{10}-helix portion is more exposed than the β-sheet core.[18]

Table 1. Crystallographic statistics for the refinement of Shp^{180}

	Refined Shp^{180} structure	Phasing data structure
Data collection		
Resolution range (Å)	41.2–2.10 (2.16-2.10)	70.7–2.60 (2.66–2.60)
Space group	$P6_5$	$P6_5$
Unit cell dimensions (Å)	$a=b=82.3$, $c=106.5$ $\alpha=\beta=90°$, $\gamma=120°$	$a=b=81.7$, $c=106.8$ $\alpha=\beta=90°$, $\gamma=120°$
Total/unique reflections	255,892/23,738	233,365/12,195
Completeness (%)	99.6 (95.3)	96.8 (73.3)
Average $I/\sigma I$	20.4 (2.3)	21.8 (2.4)
Redundancy	10.8 (7.1)	19.2 (5.1)
R_{merge}	0.115	0.129
Phasing statistics		(40.9–2.60 Å)
FOM_{acen}/FOM_{cen}	–	0.30/0.09
Phasing $power_{acen}$	–	0.87
R_{cullis}	–	0.87
Refinement statistics		
R_{work}	16.3 (22.1)	–
R_{free}	22.2 (30.7)	–
r.m.s.d. bond length (Å)	0.009	–
Coordinate error (maximum likelihood, Å)	0.12	–
Average protein *B*-value (Å^2)	28.2	–
Average hemin *B*-value (Å^2)	26.0	–
Average water *B*-value (Å^2)	39.4	–
Average ion *B*-value (Å^2)	52.3	–
No. of protein molecules/atoms	2/2344	–
No. of auxiliary molecules	4 hemin	–
No. of water molecules	323	–
No. of ions	9	–
Ramachandran plot (residues)		
In most favored (%)	94.1	–
In allowed (%)	5.9	–
In generously allowed (%)	0.0	
In disallowed (%)	0.0	
Overall *G*-factor	0.08	
PDB ID	2Q7A	–

Statistics listed in parentheses are for those reported in the last refinement shell listed in the resolution range.

Details of the heme-binding site

In addition to coordination to the sulfur atoms of Met66 and Met153, the hemin is surrounded by hydrophobic residues, which include Leu62, Val67, Leu93, Val150, Pro152, Val157, and Phe159. Within the same Shp^{180} monomer, one hemin propionate O atom is hydrogen bonded to N2 and N^{ε} of Arg155 (3.1 Å and 2.9 Å; Figure 2(a)) and to two water molecules (2.7 Å each), but remains solvent exposed. One propionate in IsdC and IsdA also hydrogen bonds to the backbone and side-chain atoms, but remains exposed to the solvent.[18,19] The other O atom of the bound heme propionate is coordinated to the exposed iron of the exogenously bound hemin dimer located at the interface between the two Shp^{180} molecules. The Fe–O bond lengths for the latter interactions are 3.0 Å and 2.9 Å for the two Shp^{180} molecules (Figure 2(b)). The exogenous hemins are stacked in a dimer and related by a 2-fold axis (Figure 2(b) and (c)), forming a structure similar to previously reported hemin dimers in aqueous solution.[34] The propionate groups of the exogenous hemin dimer form hydrogen bonds with several water molecules and Asn127 (2.7 Å). The pyrrole nitrogen atoms of the hemin dimer are located within 3.6 Å of each partner's iron atom, and these exogenous heme irons are located 4.1 Å from one another (Figure 2(b)). The packing of the exogenous hemin dimer and the protein-bound hemin is similar to the structure of β-hematin where the propionate of one hemin coordinates to the iron of another hemin (Figure 2(c)).[35,36]

Excluding the exogenous hemin dimer–protein interface, the surface contact area in the interface between the two Shp^{180} monomers is only ~276 Å^2. The exogenous hemin dimer increases the contact area between the two protein monomers by a factor of ~2 to an area of ~600 Å^2 and clearly stabilizes the

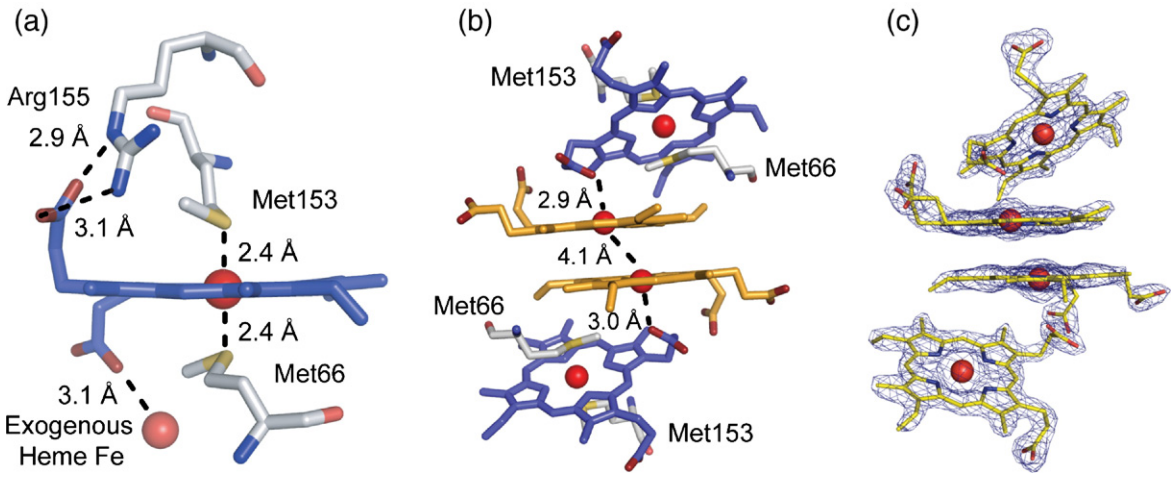


Figure 2. Bis-methionyl coordination in Shp^{180} and hemin stacking in the crystallization interface. (a) Coordination of the protein-bound heme by Met66 and Met153 in Shp^{180}. Distances between the sulfur atom (in yellow) and heme iron (sphere) are listed. Hydrogen bond distances between Arg155 and a propionate are shown and the coordination distance between the propionate and the exogenous heme iron is shown. (b) The crystallographic hemin packing between the bound hemes (blue) and the exogenous hemins (orange). Distances between the bound propionate oxygen (red) and the exogenous hemin iron atom (sphere) and the distance between the two exogenous hemin irons are shown. (c) Electron density of the protein-bound and exogenous hemins at 1.5σ using the orientation from (b). The hemins are displayed in yellow.

crystallization dimer interface. Tyr96 hydrogen bonds to the symmetry related Tyr96 at a distance of 2.4 Å near the exogenous hemin dimer, further strengthening the interface.

Analysis of the redox and oligomeric state of Shp and Shp^{180}

Spectroscopic analysis of the Shp^{180} crystals revealed a peak at 420 nm indicating that the protein is in the oxidized state.[16] The crystals also showed a lower than expected ratio between the 420 nm peak (bis-Met coordinated hemichrome) and the 370 nm peak (aqueous hemin) compared to that of oxidized Shp^{180} in solution, consistent with the presence of an extra "free" hemin in the crystals (Figure 3(a)).

Calibrated gel filtration and sedimentation velocity ultracentrifugation results indicate that the reduced and oxidized forms of holoShp^{180} exist as a monomer in solution, with both experiments yielding molecular weights (MWs) between 14 and 16 kDa (Figure 3(b) and (c)). These results are consistent with the calculated MW of 17.2 kDa for heme-bound Shp^{180}. Gel filtration results for full-length oxidized and reduced holoShp suggest a MW of ~40 kDa, which is significantly larger than the calculated value of 25.9 kDa (Figure 3(b)). In contrast, the sedimentation velocity results gave a smaller than expected S-value (2.3 *s*), which assuming spherical geometry predicts a MW for full-length Shp of only 20 kDa (Figure 3(c)). Combined, these results strongly suggest that both Shp and Shp^{180} are monomeric in aqueous solution and that Shp^{180} appears to be globular. In contrast, full-length Shp is elongated and rod-like with a larger than expected exclusion volume and frictional coefficient, which is also seen in ultracentrifugation studies of IsdA.[37] The larger exclusion volume of the rod shape explains the larger than expected apparent MW for full-length Shp obtained from the gel filtration experiment, and the larger frictional coefficient explains the smaller S-value and MW calculated from the sedimentation velocity experiments.

Structural homology

Shp^{180} does not share significant amino acid sequence similarity with the heme-binding NEAT domain proteins.[20] However, it does share the immunoglobulin-like structural fold associated with *S. aureus* surface heme-uptake proteins, IsdC,[18] IsdA,[19] and IsdH.[17] Even with sequence identities of 19% and 17%,[38] the structural alignment of carbon α-atoms between Shp^{180} and IsdC and between Shp^{180} and IsdA show an r.m.s. deviation of 2.0 Å and 2.2 Å, respectively. These values are typical r.m.s. deviations between proteins sharing the same structural fold, but less than 20% sequence identity.[27] An overlay of Shp^{180} and IsdC shows that the most significant differences are mainly confined to their loop regions (Figure 4(a)). Unlike IsdC, Shp^{180} does not contain a 3_{10}-helical lip distal to the heme, but instead has a longer α-helix where Met66 coordinates the heme iron (arrow in Figure 4(a)–(c)). The heme solvent exposure of Shp^{180} is 29%, compared to 34% for IsdC and 35% for IsdA. The protein-bound hemin in Shp^{180} is rotated 90° in relation to the bound hemin in IsdC and IsdA (Figure 4(b) and (c)). The small decrease in solvent exposure is likely due to the coordination of the iron by the second axial methionine residue. There is a large diversity among the amino acid sequences of Shp^{180} and NEAT domain proteins, and a search through FFAS03,[39] a peptide-profile sequence alignment tool,

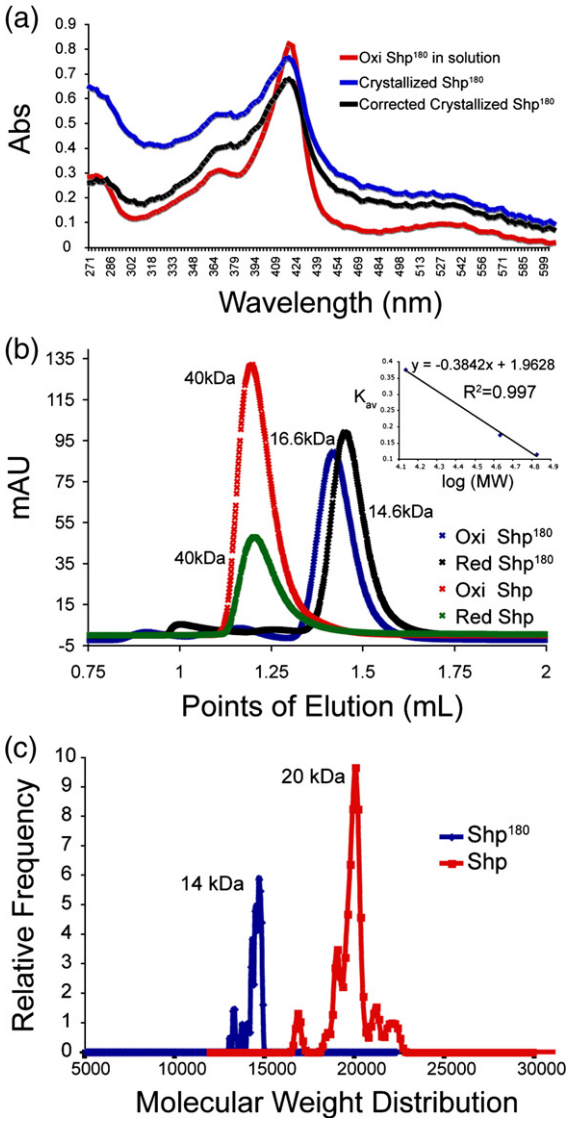


Figure 3. Spectroscopic, gel-filtration, and ultracentrifugation analysis of Shp^{180} and Shp. (a) Spectroscopic scan of oxidized Shp^{180} in solution (Oxi Shp^{180}) and crushed crystals in mother liquor (crystallized Shp^{180}). An additional scan of the Shp^{180} crystals corrected for Rayleigh scattering is shown (corrected crystallized Shp^{180}). (b) Elution of oxidized (Oxi) and reduced (Red) Shp^{180} and Shp. Molecular weights are listed next to their respective plots. The standard curve used to calculate the molecular weights and correlation coefficient is shown in the upper right. (c) Molecular weight distribution results obtained from sedimentation velocity experiments with oxidized Shp^{180} (blue) and Shp (red), as described in Materials and Methods. Molecular weights peaks are labeled.

indicates that an amino acid sequence motif for cell surface heme-binding proteins in Gram-positive bacteria is undefinable at present.

Surface charge distribution

The electrostatic properties of Shp and IsdC were examined. The calculated isoelectric point (pI)[40] of Shp and the heme-binding portion of Shp^{180} are 5.3 and 4.6, respectively, whereas the calculated pI of Shr is 8.7. Similarly, IsdA has a calculated pI of 9.1, whereas IsdC has a calculated pI of 6.6, and again the two heme transport pathway components have opposite charges under physiological conditions. These observations suggest that favorable electrostatic interactions may facilitate the formation of bimolecular protein complexes to facilitate unimolecular heme transfer. This type of facilitated transfer mechanism is observed for the reaction of holoShp with apoHtsA.[16,26] Interestingly, although both Shp^{180} and IsdC are acidic proteins, they differ in the electrostatic surface around their heme-binding pockets. Shp^{180} displays a large electronegative ring around the heme-binding site (Figure 4(d)). Favorable electrostatic interactions between proteins are often found to drive complex formation in nature[41] and the negative ring surrounding the Shp^{180} heme pocket may present a potential binding site with the more basic Shr. In contrast, IsdC does not have a negative ring around the bound heme, but shows dispersed positive and negative patches (Figure 4(e)).

Discussion

We have solved the structure of the heme-binding domain of Shp, a protein that transfers its heme to HtsA. The C37S mutation in Shp^{180} was used to facilitate crystal formation by avoiding potential oxidation of the Cys residue during the crystallization process. The C37S residue is 23.9 Å away from the heme iron atom in the middle of β-strand B1 (Figure 1) and does not cause an alteration in heme transfer rate or mechanism of Shp^{180}. Truncated Shp^{180} binds heme, has the same EPR and UV-visible spectral properties as full-length Shp, and retains the ability to rapidly transfer both hemin and heme to apoHtsA by the activated ternary complex mechanism that is observed for the full-length Shp-apoHtsA reactions.[26] Thus, the structure of Shp^{180} provides valuable information for understanding the mechanisms of hemin transfer by the full-length cell surface protein.

Shp^{180} has the immunoglobulin-like β-sandwich fold that is found in the NEAT domain of *S. aureus* IsdA, IsdH, and IsdC. The heme is located in the cavity formed by the single α-helix and β-strands B7 and B8 in Shp^{180} (Figure 1), an arrangement that is similar to those in IsdA and IsdC. The oligomeric studies revealed that Shp^{180} has an overall elongated protein structure, also seen in IsdA. In addition, like the *S. aureus* proteins, the bound hemin in Shp^{180} has significant solvent exposure.[18] Shp was excluded from the NEAT family by Andrade *et al.* who referred to Shp as Spy1796.[20] The homology in amino acid sequence between Shp^{180} and the NEAT domain of IsdA or IsdC (17%–19% identity) is similar to that between the IsdA and IsdC NEAT domains (19% identity),[38] suggesting that Shp is at least a distant member of the NEAT family. Thus, the two distinct heme acquisition

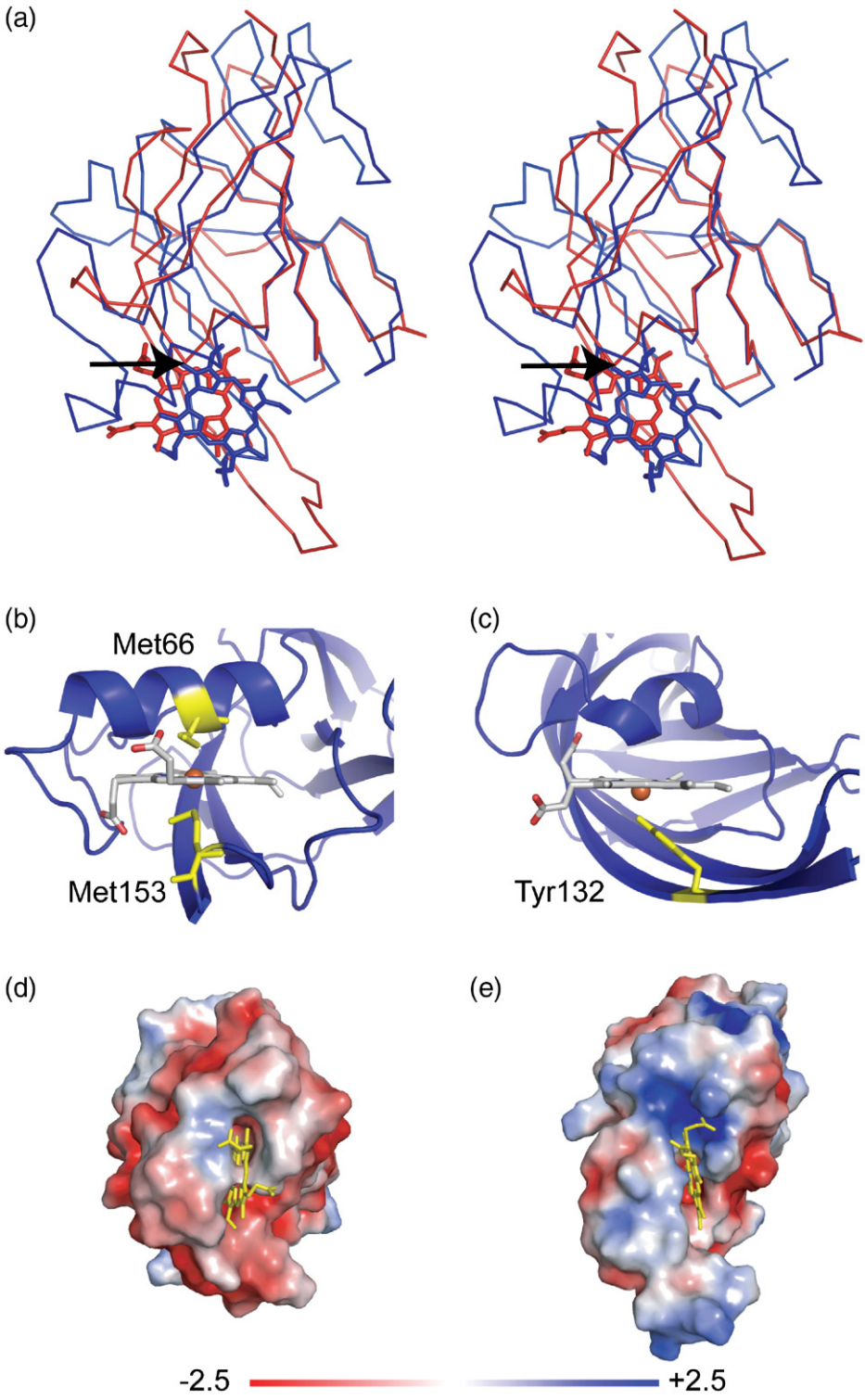


Figure 4. Structural comparisons of Shp^{180} and IsdC proteins. (a) Stereo image of the C^{α} trace between Shp^{180} (blue) and IsdC (red, PDB ID 2O6P). The arrow points to differences between the longer α-helix Shp^{180} where Met66 coordinates one side of the heme and the shorter 3_{10}-helical lip of IsdC. (b) and (c) Heme pockets of Shp^{180} (b) and IsdC (c). The proteins are shown in blue, the residues that coordinate to the heme are labeled and shown in yellow, and the hemes are in gray. (d) and (e) Electrostatic surface potential of the Shp^{180} (d) and IsdC (e) proteins. Electrostatic surface potentials were calculated (keV) in the presence of 140 mM monovalent salt concentration at 310 K. The hemins are shown in yellow for both Shp^{180} and IsdC.

systems may have evolved from the same ancestor through divergence; in addition, HtsA shares 40% identity in amino acid sequence with IsdE from *S. aureus*,[15,24] further supporting the divergence theory. The structural similarities between Shp and IsdA/C and homology between HtsA and IsdE

suggest that heme uptake and transfer into *S. aureus* and *S. pyogenes* proteins may follow similar molecular mechanisms and that parallel functions exist for the two systems. For example, Shr and IsdB may acquire hemin from hemoglobin, and Shp and IsdA/C may relay hemin from Shr and IsdB to HtsA and IsdE, respectively.

The heme iron of Shp is coordinated to Met66 and Met153; Met66 is more exposed to the solvent than Met153, suggesting that the Met153 side is more important for the affinity of Shp for hemin. Bis-methionine coordination was previously observed between two monomers in bacterioferritin.[42] The bis-methionyl coordination in Shp is unique because it is the first example of heme iron corrdination to two methionine residues in the same protein monomer. In contrast, the heme iron is ligated to a Tyr residue in IsdA, IsdC, and ChaN, a His residue in HemS, and His and Tyr residues in HasA. Single Ala replacements of Met66 and Met153 in full-length Shp cause formation of pentacoordinate hemin–Met complexes and slower rates of heme transfer, and Met153, but not Met66, is critical to maintaining the high affinity of Shp for hemin.[26] The structure of Shp^{180} supports these observations. Furthermore, bis-methionine coordination in Shp is critical for its rapid hemin transfer to apoHtsA.[26] These observations suggest that although the basic mechanism of transfer between receptor proteins in bacterial heme acquisition may be the same, the structural details of iron coordination are not strictly conserved.

The heme and hemin transfer from Shp to HtsA involves the displacement of the two Met ligands in Shp with two ligands from apoHtsA, His229 and Met79 (B. Lei *et al.*, unpublished data). After formation of the binary protein complex, Shp-to-HtsA heme and hemin transfers show only one first-order kinetic phase, indicating that the displacement of the first Shp Met ligand is rate-limiting. In either case, the two new coordination bonds are formed at effectively the same time. Thus, the two axial ligands of apoHtsA must be close to the two axial positions of hemin in the holoShp–apoHtsA binary complex, requiring that the HtsA axial side-chains can easily access the hemin ring in Shp. The bound hemin in Shp^{180} has significant exposure to solvent on both Met153 and Met66 sides. Thus, simultaneous ligand displacement by adjacent apoHtsA ligands in a Shp–HtsA complex is structurally feasible by sliding movements of the amino acid side-chains of apoHtsA across both sides of the hemin plane. The hemin in HasA, IsdA, and IsdC are also significantly exposed to solvent on both sides of the hemin ring, suggesting that hemin transfer by these proteins may use mechanisms similar to the sliding mechanism proposed here for the reaction of holoShp with apoHtsA.

Like bacterioferritin,[42] Shp shows a weak absorbance peak at 370 nm, which is often associated with free hemin, but pyridine hemochromagen and iron analysis show only one heme per Shp monomer. However, when Shp^{180} was crystallized, a significant increase in the ratio of the peak at 370 nm to that at 420 nm is observed, suggesting that the crystallized protein has acquired additional, "free" hemin. During crystallization, a portion of Shp^{180} precipitated in the hanging-drops within days, and crystals only formed weeks later. It is likely that the protein precipitation facilitates the release of hemin, which dimerizes[34] and then nucleates crystallization of Shp^{180} dimers. This apparent requirement for exogenous hemin in the crystal packing may explain the slow rate of crystal growth. The interface between the two molecules of Shp^{180}, as observed in the crystal structure, is held together primarily by the exogenous hemin dimer, where the porphyrin rings provide the majority of the contact area, ~334 $Å^2$ of the 600 $Å^2$ interface. This situation is also seen in the periplasmic protein, ChaN, where the co-facial protein-bound hemes account for 380 $Å^2$ of the 680 $Å^2$ dimer interface.[22]

Gel filtration and ultracentrifugation studies indicate that both Shp^{180} and Shp are monomers in solution and that the truncated hemin-binding domain is globular, whereas the full-length protein has a rod-like shape. However, full-length Shp could in principle bind exogenous hemin dimers, perhaps after massive red blood cell lysis and hemoglobin denaturation, and then transiently form a dimer on the cell surface of *S. pyogenes* as a mechanism for sequestering even more heme for iron metabolism. These extra "free" hemins might then be taken up passively by apoHtsA or by apoShp after it is transferred its bound hemin to the membrane transporter. However, at present there is no evidence for these more indirect uptake processes.

The exogenous hemin stacking arrangement in the crystals could also represent a mechanism comparable to β-hematin pigment formation in *Plasmodium* malarial bacteria.[35,36] This protozoan parasite is able to sequester free heme by stacking rings through the interactions of adjacent propionates, which creates a complex that is relatively inert and incapable of generating radical oxygen species (ROS) that could kill the organism. Similar problems with excess free hemin may occur after massive lysis of red cells and Heinz body formation induced by hemolysin activities during infection.

Shp^{180} has a high sequence homology (75% identity and 91% similarity) to the N-terminal portion of the *Streptococcus equi* homolog SeShp.[43] *S. equi* causes strangles, an extremely infectious disease of the upper respiratory tract in horses.[44] Proteins involved in the heme-uptake pathway appear to be conserved in *S. pyogenes* and *S. equi*.[43] From high sequence identity between the proteins of *S. equi and S. pyogenes*, it is highly probable that SeShp shares the immunoglobulin-like β-sandwich fold and that the heme-binding portion is located in the N-terminal region with bis-methionyl coordination. Thus, it is highly likely that the same heme uptake and transport mechanisms occur in these closely related pathogens.

Materials and Methods

Cloning and protein purification

Shp^{180} contains amino acid residues 30–180 of Shp. The amplification of the truncated DNA product was created by using PCR primers 5′-ACCATGGATAAAGGTCAA-ATTTATGGATG-3′ and 5′-CGAATTCAAGTAACAAGC-TGGGCCAAC-3′ from the *shp* gene clone pSHP that was originally cloned from strain MGAS5005.[2] The truncated Shp^{180} PCR product was inserted into a pET-21d (Novagen, Madison, WI) plasmid at the NcoI and EcoRI sites, yielding recombinant plasmid $pSHP^{180}$. In order to improve expression levels, a C37S mutation was incorporated and obtained by site-directed mutagenesis using $pSHP^{180}$, a QuickChange site-directed mutagenesis kit (Stratagene, La Jolla, CA), and primers 5′-AAAGGTCA-AATTTATGGATCTATTATTCAAAGAAATTAT-3′ and 5′-ATAATTTCTTTGAATAATAGATCCATAAATTTGAC-CTTT-3′, yielding $pSHP^{180C37S}$. The mutated truncated *shp* gene was sequenced to confirm the desired mutation.

Shp^{180} was expressed in *E. coli* BL21(DE3) containing $pSHP^{180C37S}$, with the majority of the expressed protein in inclusion bodies. After expression, the cell pellet was resuspended in ice-cold 50 ml Tris–HCl (pH 8.0) and sonicated in 1s bursts for 15 min on ice, followed by centrifugation at 20,000*g* for 15 minutes. The Shp^{180} inclusion body was dissolved in 50 ml of 8 M urea. The denatured protein was refolded by diluting 40-fold with 20 mM Tris–HCl (pH 8.0) containing excess hemin (using a 1.5-fold hemin to protein ratio). The refolded heme-bound Shp^{180} was loaded onto a DEAE column (2.5 cm × 10 cm), and the column was washed with 100 ml of 20 mM Tris–HCl (pH 8.0) and eluted with a 100 ml linear gradient of 0–0.25 M NaCl at room temperature. The Shp^{180} solution was adjusted to 0.8 M $(NH_4)_2SO_4$, 20 mM Tris–HCl at pH 8.0 (buffer) and loaded onto a phenyl Sepharose column (1.5 cm × 6 cm), washed with 100 ml of buffer B, and eluted with a 100-ml linear gradient of buffer B to buffer A (20 mM Tris–HCl, pH 8.0) at room temperature. Shp^{180} was dialyzed against buffer A and concentrated using Centricon Plus 20 filtration devices (Millipore, Bedford, MA).

Crystallization conditions

Crystals were grown by the hanging-drop vapor-diffusion method with 0.8 M ammonium sulfate and 0.1 M Mes (pH 6.0) using 70 mg ml^{-1} Shp^{180} in 20 mM Tris (pH 8.0). Hanging drops consisted of 1 μl of protein solution mixed with 1 μl of reservoir solution. Red diffraction quality crystals grew to ~20 μm × 50 μm × 100 μm needles within two months at 295 K. Shp^{180} crystals were cryo-protected in a single step using 0.9 M ammonium sulfate, 30% (v/v) glycerol, and 0.1 M Mes (pH 6.0) and flash-cooled in liquid nitrogen.

Structure determination

X-ray diffraction data used for initial phasing were collected at the Life Sciences Collaborative Access Team (LS-CAT) Sector 21ID-D beamline at the Advanced Photon Source (Argonne National Laboratories, Argonne, IL). Data were collected at a wavelength of 1.6531 Å at 100K and diffraction images were integrated and scaled to a resolution of 2.6 Å using HKL2000.[45] The iron substructure of Shp^{180} was determined using HySS[46] and Shp^{180} was phased using autoSHARP,[47] which uses multiple auxiliary programs from the CCP4 suite.[48] The starting backbone model was partially built (~75% of the two chains in the asymmetric unit) with ARP/wARP[49] and the remaining model and side-chains were built manually in Coot[50] and refined in REFMAC5.[51] A higher resolution X-ray diffraction data set was collected at the General Medicine and Cancer Institutes Collaborative Access Team (GM/CA-CAT) Sector 23ID-D beamline at the Advanced Photon Source. Data were collected at a wavelength of 0.9793 Å at 100K and diffraction images were integrated and scaled to a resolution of 2.1 Å using HKL2000.[45] The 2.1 Å Shp^{180} structure was determined using molecular replacement with the previous 2.6 Å Shp^{180} structure in MolRep.[52] The model was manually fitted in Coot[50] and refined in REFMAC5.[51]

Spectroscopic analysis, ultracentrifugation, and size-exclusion chromatography

Before the proteins were analyzed by gel-filtration chromatography, the reduced (containing iron(II)) and oxidized (containing iron(III)) forms were verified spectroscopically for peaks at 428 nm and 420 nm, respectively.[16] Spectroscopic scans of Shp^{180} crystals were made using an ND-1000 spectrophotometer (NanoDrop, Wilmington, DE) from crushed crystals in 2 μl of mother liquor. Spectroscopic scans of the Shp^{180} crystals were manually corrected for Rayleigh scattering as follows:

$$Abs_{\text{corrected}} = Abs_{\lambda} - (x)(\lambda_{\text{nm}}{}^{y}) \quad (1)$$

where x is the linear and y are the exponential scattering coefficients. From the Shp^{180} crystal spectroscopic scans, x and y were estimated to be 2.4×10^7 and 3.45, respectively. The reduced and oxidized form of Shp^{180} and Shp were analyzed on a calibrated gel filtration Superdex 75 PC 3.2/30 column (GE Healthcare, Piscataway, NJ) in 20 mM Tris (pH 8.0). The reduced and oxidized form of Shp^{180} and the oxidized form of Shp were run using 150 μM protein. The reduced form of Shp was run at 40 μM. Flow rate was kept at 0.04 ml min^{-1} for the size-exclusion experiments. Sedimentation velocity experiments were performed using oxidized Shp^{180} and Shp at 150 μM in 20 mM Tris (pH 8.0), 25 °C in a Beckman model XLA centrifuge at a rotor speed of 60,000 rpm. Data were analyzed for s value and MW distributions (assuming spherical geometry, $\bar{V}$bar = 0.722 cm^3 g^{-1}) using Ultrascan 9.0 (University of Texas at San Antonio, San Antonio, TX).

Surface area and root mean squared deviation calculations

The solvent accessible surface area of the Shp^{180} heme and crystallographic dimer crystallization packing surface areas were calculated using AREAIMOL.[53] The percentage of heme surface area exposure was calculated using 825 $Å^2$ as the free heme area.[18] r.m.s. deviations between selected protein structures were calculated in VMD.[54] The structural assignments involved aligning 98 Shp^{180} residues out of 122 (~80%) with 123 residues of IsdC and 100 Shp^{180} residues out of 122 (~82%) with 121 residues of IsdA. Electrostatic surface potentials of Shp^{180} and IsdC were calculated using APBS.[55] Figures were prepared in PyMOL†.

† http://pymol.sourceforge.net/

Protein Data Bank accession code

The atomic coordinates of Shp^{180} were deposited in the RCSB Protein Data Bank[32] under the accession number 2Q7A.

Acknowledgements

This work was supported by the National Institutes of Health grants 5 T32 GM08349 (to R. A.), K22 AI057347 (to B.L.), R01 GM035469 (to J. S.O.), and R01 HL47020 (to J.S.O.), the National Center for Research Resources grant P20 RR-020185 (to B.L.), the National Institutes of Health Protein Structure Initiative U54 GM0749011 (to E.B. and G.N.P.), the Montana State University Agricultural Experimental Station (to B.L.), and the Robert A. Welch Foundation Grant C0612. GM/CA-CAT has been funded in whole or in part with Federal funds from the National Cancer Institute (Y1-CO-1020) and the National Institute of General Medical Science (Y1-GM-1104). Use of the LS-CAT Sector 21 was supported by the Michigan Economic Development Corporation and the Michigan Technology Tri-Corridor for the support of this research program (grant 085P1000817). Use of the Advanced Photon Source was supported by the US Department of Energy, Basic Energy Sciences, Office of Science, under contract no. DE-AC02-06CH11357 (GM/CA-CAT) and no. DE-AC02-06CH11357 (LS-CAT). We are appreciative of the access to crystallization equipment and X-ray facilities at the Center for Eukaryotic Structural Genomics (CESG) and to the ND-1000 Spectrophotometer in the laboratory of Dr Judith E. Kimble at the University of Wisconsin-Madison. Thanks to Dr Craig A. Bingman for crystallographic support (CESG), Ryan M. Bannen (Department of Biochemistry, University of Wisconsin-Madison) for helping with the calibrated gel filtration experiments, and Elena J. Levin and Christopher M. Bianchetti (Department of Biochemistry, University of Wisconsin-Madison) for useful discussions.

References

1. Mazmanian, S. K., Skaar, E. P., Gaspar, A. H., Humayun, M., Gornicki, P., Jelenska, J. *et al.* (2003). Passage of heme-iron across the envelope of *Staphylococcus aureus*. *Science*, **299**, 906–909.
2. Lei, B., Smoot, L. M., Menning, H. M., Voyich, J. M., Kala, S. V., Deleo, F. R. *et al.* (2002). Identification and characterization of a novel heme-associated cell surface protein made by *Streptococcus pyogenes*. *Infect. Immun.* **70**, 4494–4500.
3. Field, L. H., Headley, V. L., Payne, S. M. & Berry, L. J. (1986). Influence of iron on growth, morphology, outer membrane protein composition, and synthesis of siderophores in *Campylobacter jejuni*. *Infect. Immun.* **54**, 126–132.
4. Wooldridge, K. G. & Williams, P. H. (1993). Iron uptake mechanisms of pathogenic bacteria. *FEMS Microbiol. Rev.* **12**, 325–348.
5. Weinberg, E. D. (1978). Iron and infection. *Microbiol. Rev.* **42**, 45–66.
6. Otto, B. R., Verweij-van Vught, A. M. & MacLaren, D. M. (1992). Transferrins and heme-compounds as iron sources for pathogenic bacteria. *Crit. Rev. Microbiol.* **18**, 217–233.
7. Rouault, T. A. (2004). Microbiology. Pathogenic bacteria prefer heme. *Science*, **305**, 1577–1578.
8. Skaar, E. P., Humayun, M., Bae, T., DeBord, K. L. & Schneewind, O. (2004). Iron-source preference of *Staphylococcus aureus* infections. *Science*, **305**, 1626–1628.
9. Stojiljkovic, I. & Perkins-Balding, D. (2002). Processing of heme and heme-containing proteins by bacteria. *DNA Cell Biol.* **21**, 281–295.
10. Musser, J. M. & Krause, R. M. (1998). The revival of group A streptococcal disease with a commentary on staphylococcal toxic shock syndrome. In *Emerging Infections* (Krause, R. M. & Fauci, A., eds), Academic Press, San Diego, CA.
11. Francis, R. T., Jr, Booth, J. W. & Becker, R. R. (1985). Uptake of iron from hemoglobin and the haptoglobin-hemoglobin complex by hemolytic bacteria. *Int. J. Biochem.* **17**, 767–773.
12. Eichenbaum, Z., Muller, E., Morse, S. A. & Scott, J. R. (1996). Acquisition of iron from host proteins by the group A streptococcus. *Infect. Immun.* **64**, 5428–5429.
13. Bates, C. S., Montanez, G. E., Woods, C. R., Vincent, R. M. & Eichenbaum, Z. (2003). Identification and characterization of a *Streptococcus pyogenes* operon involved in binding of hemoproteins and acquisition of iron. *Infect. Immun.* **71**, 1042–1055.
14. Lei, B., Liu, M., Voyich, J. M., Prater, C. I., Kala, S. V., DeLeo, F. R. & Musser, J. M. (2003). Identification and characterization of HtsA, a second heme-binding protein made by *Streptococcus pyogenes*. *Infect. Immun.* **71**, 5962–5969.
15. Liu, M. & Lei, B. (2005). Heme transfer from streptococcal cell surface protein Shp to HtsA of transporter HtsABC. *Infect. Immun.* **73**, 5086–5092.
16. Nygaard, T. K., Blouin, G. C., Liu, M., Fukumura, M., Olson, J. S., Fabian, M. *et al.* (2006). The mechanism of direct heme transfer from the streptococcal cell surface protein Shp to HtsA of the HtsABC transporter. *J. Biol. Chem.* **281**, 20761–20771.
17. Pilpa, R. M., Fadeev, E. A., Villareal, V. A., Wong, M. L., Phillips, M. & Clubb, R. T. (2006). Solution structure of the NEAT (NEAr Transporter) domain from IsdH/HarA: the human hemoglobin receptor in *Staphylococcus aureus*. *J. Mol. Biol.* **360**, 435–447.
18. Sharp, K. H., Schneider, S., Cockayne, A. & Paoli, M. (2007). Crystal structure of the heme-IsdC complex, the central conduit of the Isd Iron/heme uptake system in *Staphylococcus aureus*. *J. Biol. Chem.* **282**, 10625–10631.
19. Grigg, J. C., Vermeiren, C. L., Heinrichs, D. E. & Murphy, M. E. (2007). Haem recognition by a *Staphylococcus aureus* NEAT domain. *Mol. Microbiol.* **63**, 139–149.
20. Andrade, M. A., Ciccarelli, F. D., Perez-Iratxeta, C. & Bork, P. (2002). NEAT: a domain duplicated in genes near the components of a putative Fe^{3+} siderophore transporter from Gram-positive pathogenic bacteria. *Genome Biol.* **3**; RESEARCH0047.
21. Arnoux, P., Haser, R., Izadi, N., Lecroisey, A., Delepierre, M., Wandersman, C. & Czjzek, M. (1999). The crystal structure of HasA, a hemophore

secreted by *Serratia marcescens*. *Nature Struct. Biol.* **6**, 516–520.
22. Chan, A. C. K., Lelj-Garolla, B., Rosell, F. I., Peterson, K. A., Mauk, A. G. & Murphy, M. E. P. (2006). Cofacial heme binding is linked to dimerization by a bacterial heme transport protein. *J. Mol. Biol.* **362**, 1108–1119.
23. Schneider, S., Sharp, K. H., Barker, P. D. & Paoli, M. (2006). An induced fit conformational change underlies the binding mechanism of the heme transport proteobacteria-protein HemS. *J. Biol. Chem.* **281**, 32606–32610.
24. Grigg, J. C., Vermeiren, C. L., Heinrichs, D. E. & Murphy M. E. (2007). Heme coordination by *Staphylococcus aureus* IsdE. *J. Biol. Chem.* doi:10.1074/jbc.M704602200, In the press.
25. Suits, M. D., Jaffer, N. & Jia, Z. (2006). Structure of the *Escherichia coli* O157:H7 heme oxygenase ChuS in complex with heme and enzymatic inactivation by mutation of the heme coordinating residue His-193. *J. Biol. Chem.* **281**, 36776–36782.
26. Ran, Y., Zhu, H., Liu, M., Fabian, M., Olson, J.S., Aranda, R. *et al.* (2007). Bis-methionine ligation to heme iron in the streptococcal cell surface protein Shp facilitates rapid hemin transfer to HtsA of the HtsABC transporter. *J. Biol. Chem.* doi:10.1074/jbc.M705967200, In the press.
27. Chothia, C. & Lesk, A. M. (1986). The relation between the divergence of sequence and structure in proteins. *EMBO J.* **5**, 823–826.
28. Cheesman, M. R., Thomson, A. J., Greenwood, C., Moore, G. R. & Kadir, F. (1990). Bis-methionine axial ligation of haem in bacterioferritin from *Pseudomonas aeruginosa*. *Nature*, **346**, 771–773.
29. Cobessi, D., Huang, L. S., Ban, M., Pon, N. G., Daldal, F. & Berry, E. A. (2002). The 2.6 Å resolution structure of Rhodobacter capsulatus bacterioferritin with metal-free dinuclear site and heme iron in a crystallographic 'special position'. *Acta Crystallog. sect. D*, **58**, 29–38.
30. Frolow, F., Kalb, A. J. & Yariv, J. (1994). Structure of a unique twofold symmetric haem-binding site. *Nature Struct. Biol.* **1**, 453–460.
31. Swartz, L., Kuchinskas, M., Li, H., Poulos, T. L. & Lanzilotta, W. N. (2006). Redox-dependent structural changes in the *Azotobacter vinelandii* bacterioferritin: new insights into the ferroxidase and iron transport mechanism. *Biochemistry*, **45**, 4421–4428.
32. Berman, H. M., Westbrook, J., Feng, Z., Gilliland, G., Bhat, T. N., Weissig, H. *et al.* (2000). The Protein Data Bank. *Nucl. Acids Res.* **28**, 235–242.
33. Harding, M. M. (2006). Small revisions to predicted distances around metal sites in proteins. *Acta Crystallog. sect. D*, **62**, 678–682.
34. de Villiers, K. A., Kaschula, C. H., Egan, T. J. & Marques, H. M. (2007). Speciation and structure of ferriprotoporphyrin IX in aqueous solution: spectroscopic and diffusion measurements demonstrate dimerization, but not mu-oxo dimer formation. *J. Biol. Inorg. Chem.* **12**, 101–117.
35. Carney, C. K., Schrimpe, A. C., Halfpenny, K., Harry, R. S., Miller, C. M., Broncel, M. *et al.* (2006). The basis of the immunomodulatory activity of malaria pigment (hemozoin). *J. Biol. Inorg. Chem.* **11**, 917–929.
36. Pagola, S., Stephens, P. W., Bohle, D. S., Kosar, A. D. & Madsen, S. K. (2000). The structure of malaria pigment beta-haematin. *Nature*, **404**, 307–310.
37. Vermeiren, C. L., Pluym, M., Mack, J., Heinrichs, D. E. & Stillman, M. J. (2006). Characterization of the heme binding properties of *Staphylococcus aureus* IsdA. *Biochemistry*, **45**, 12867–12875.
38. Thompson, J. D., Higgins, D. G. & Gibson, T. J. (1994). CLUSTAL W: improving the sensitivity of progressive multiple sequence alignment through sequence weighting, position-specific gap penalties and weight matrix choice. *Nucl. Acids Res.* **22**, 4673–4680.
39. Jaroszewski, L., Rychlewski, L., Li, Z., Li, W. & Godzik, A. (2005). FFAS03: a server for profile–profile sequence alignments. *Nucl. Acids Res.* **33**, W284–W288.
40. Gasteiger, E., Hoogland, C., Gattiker, A., Duvaud, S., Wilkins, M. R., Appel, R. D. & Bairoch, A. (2005). Protein identification and analysis tools on the ExPASy server. In *The Proteomics Protocols Handbook* (Walker, J. M., ed), Humana Press, Totowa, NJ.
41. Shaul, Y. & Schreiber, G. (2005). Exploring the charge space of protein-protein association: a proteomic study. *Proteins: Struct. Funct. Genet.* **60**, 341–352.
42. Andrews, S. C., Le Brun, N. E., Barynin, V., Thomson, A. J., Moore, G. R., Guest, J. R. & Harrison, P. M. (1995). Site-directed replacement of the coaxial heme ligands of bacterioferritin generates heme-free variants. *J. Biol. Chem.* **270**, 23268–23274.
43. Nygaard, T. K., Liu, M., McClure, M. J. & Lei, B. (2006). Identification and characterization of the heme-binding proteins SeShp and SeHtsA of *Streptococcus equi* subspecies equi. *BMC Microbiol.* **6**, 82.
44. Timoney, J. F. (2004). The pathogenic equine streptococci. *Vet. Res.* **35**, 397–409.
45. Otwinowski, Z. & Minor, W. (1997). Processing of X-ray diffraction data collected in oscillation mode. *Methods Enzymol.* **276**, 307–326.
46. Grosse-Kunstleve, R. W. & Adams, P. D. (2003). Substructure search procedures for macromolecular structures. *Acta Crystallog. sect. D*, **59**, 1966–1973.
47. de la Fortelle, E. & Bricogne, G. (1997). Maximum-likelihood heavy-atom parameter refinement for multiple isomorphous replacement and multiwavelength anomalous diffraction methods. *Methods Enzymol.* **276**, 472–494.
48. PROJECT, C.C. (1994). The CCP4 Suite: programs for protein crystallography. *Acta Crystallog. sect. D*, **50**, 760–763.
49. Perrakis, A., Morris, R. & Lamzin, V. S. (1999). Automated protein model building combined with iterative structure refinement. *Nature Struct. Biol.* **6**, 458–463.
50. Emsley, P. & Cowtan, K. (2004). Coot: model-building tools for molecular graphics. *Acta Crystallog. sect. D*, **60**, 2126–2132.
51. Murshudov, G. N., Vagin, A. A. & Dodson, E. J. (1997). Refinement of macromolecular structures by the maximum-likelihood method. *Acta Crystallog. sect. D*, **53**, 240–255.
52. Vagin, A. & Teplyakov, A. (1997). MOLREP: an automated program for molecular replacement. *J. Appl. Crystallog.* **30**, 1022–1025.
53. Lee, B. & Richards, F. M. (1971). The interpretation of protein structures: estimation of static accessibility. *J. Mol. Biol.* **55**, 379–400.
54. Humphrey, W., Dalke, A., & Schulten, K. (1996). VMD: visual molecular dynamics. *J. Mol. Graph.* **14**, 33–8, 27–8.
55. Baker, N. A., Sept, D., Joseph, S., Holst, M. J. & McCammon, J. A. (2001). Electrostatics of nanosystems: application to microtubules and the ribosome. *Proc. Natl Acad. Sci. USA*, **98**, 10037–10041.